UC San Diego
UC San Diego Previously Published Works

Title

Phosphopeptidomics Reveals Differential Phosphorylation States and Novel SxE Phosphosite Motifs of Neuropeptides in Dense Core Secretory Vesicles

Permalink

https://escholarship.org/uc/item/5fj7827z

Journal

Journal of The American Society for Mass Spectrometry, 29(5)

ISSN

1044-0305

Authors

Lietz, Christopher B
Toneff, Thomas
Mosier, Charles
et al.

Publication Date

2018-05-01

DOI

10.1007/s13361-018-1915-0

Peer reviewed

Phosphopeptidomics Reveals Differential Phosphorylation States and Novel SxE Phosphosite Motifs of Neuropeptides in Dense Core Secretory Vesicles

Christopher B. Lietz[1], **Thomas Toneff**[1], **Charles Mosier**[1], **Sonia Podvin**[1], **Anthony J. O'Donoghue**[1], and **Vivian Hook**[1,2,*]

[1]Skaggs School of Pharmacy and Pharmaceutical Sciences, University of California San Diego, La Jolla, CA 92093

[2]Dept. of Neurosciences, School of Medicine, University of California San Diego, La Jolla, CA 92093

Abstract

Neuropeptides are vital for cell-cell communication and function in the regulation of the nervous and endocrine systems. They are generated by post-translational modification (PTM) steps resulting in small active peptides generated from prohormone precursors. Phosphorylation is a significant PTM for the bioactivity of neuropeptides. From the known diversity of distinct neuropeptide functions, it is hypothesized that the extent of phosphorylation varies among different neuropeptides. To assess this hypothesis, neuropeptide-containing dense core secretory vesicles from bovine adrenal medullary chromaffin cells were subjected to global phosphopeptidomics analyses by liquid chromatography (LC)-mass spectrometry (MS/MS). Phosphopeptides were identified directly by LC-MS/MS and indirectly by phosphatase treatment followed by LC-MS/MS. The data identified numerous phosphorylated peptides derived from neuropeptide precursors such as chromogranins, secretogranins, proenkephalin and pro-NPY. Phosphosite occupancies were observed at high and low levels among identified peptides and many of the high occupancy phosphopeptides represent prohormone-derived peptides with currently unknown bioactivities. Peptide sequence analyses demonstrated SxE as the most prevalent phosphorylation site motif, corresponding to phosphorylation sites of the Fam20C protein kinase known to be present in the secretory pathway. The range of high to low phosphosite occupancies for neuropeptides demonstrates cellular regulation of neuropeptide phosphorylation.

Graphical abstract

---

*Address correspondence to: Dr. Vivian Hook, Skaggs School of Pharmacy and Pharmaceutical Sciences, University of California San Diego, 9500 Gilman Dr. MC0719, La Jolla, CA 92093-0719, phone 858-822-6682, vhook@ucsd.edu.
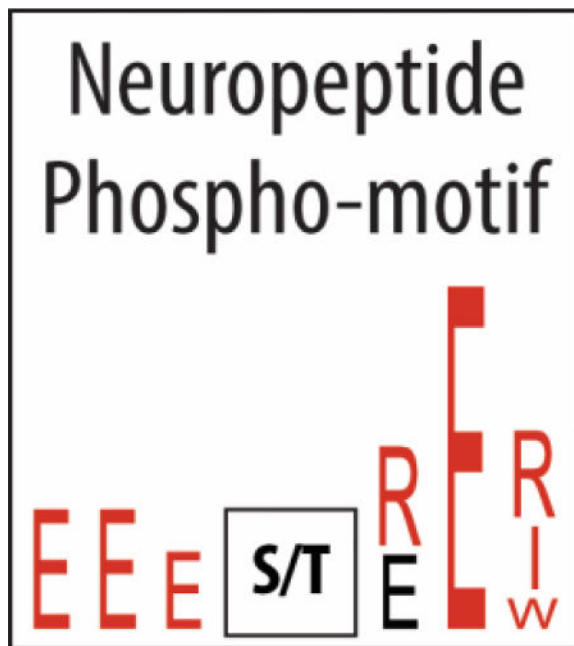
Introduction

Neuropeptides are secreted peptide signaling molecules that regulate cellular functions in the nervous and endocrine systems. They participate in diverse biological roles, ranging from neurotransmission [1] to hormonal signaling [2–6] and antimicrobial defense [7–10]. The type of activities exerted by neuropeptides is defined by their structures. Peptide sequence, post-translational modifications (PTMs), and three-dimensional properties are all significant factors for the vital neuropeptide functions in virtually all neuroendocrine processes.

Neuropeptides are generated in secretory cells by post-translational processing of their protein precursors [11–12]. Neuropeptide precursors, known as prohormones or proneuropeptides, are targeted to the rough endoplasmic reticulum during translation [13] and subsequently routed to the trans-Golgi apparatus where dense core secretory vesicles (DCSVs) are formed. DCSVs, also known as secretory granules [14], package prohormones together with processing enzymes. As DCSVs mature, occuring during axonal transport in neurons, neuropeptide precursors are converted into bioactive neuropeptides. Neural activity or secretagogue stimulation can then induce DCSV exocytosis and release of neuropeptides [11, 15–18].

Neuropeptide PTMs are important for bioactivities [19–21]. Phosphorylation, a ubiquitous molecular switch among intact proteins [22–23], is one such PTM. In neuropeptides and

prohormones, serine phosphorylation enables enkelytin's inhibition of bacterial growth [7–8], tyrosine phosphorylation regulates proteolytic processing of the gastrin precursor [24–25], and α-MSH phosphorylation reduces its binding affinity for melanocortin receptors [26].

The dynamic bioactivities of neuropeptides implicate their differential states of phosphorylation. However, there are few examples in the literature where the global extent of neuropeptide phosphorylation has been studied [16, 26–28]. Therefore, the goal of this study was to investigate the phosphorylated neuropeptidome of DCSVs with respect to the identity and phosphorylation stoichiometry of endogenous phosphopeptides, and the corresponding phosphorylation site motifs.

This study analyzed DCSVs isolated from bovine sympathoadrenal chromaffin cells of the adrenal medulla by liquid chromatography (LC)-mass spectrometry (MS)-based peptidomics [12, 29–30]. These bovine DCSVs are known to represent a neuropeptide organelle model of human DCSVs in the brain and peripheral nervous system [31–32]. Phosphosite occupancy was estimated by two methods. In one method, phosphopeptide intensity was directly compared to the intensity of its non-phosphorylated counterpart [26]. In the other method, phosphosite occupancy was inferred through the intensity changes of non-phosphorylated peptides after dephosphorylation by phosphatase [33]. High-occupancy phosphosites are often relevant to biological function [34]. The data highlighted numerous high- and low-occupancy phosphosites on peptides derived from neuropeptide precursors including chromogranins, secretogranins, proenkephalin, and pro-NPY. Phosphosite sequence motifs analyzed by iceLogo [35] indicate the prevalence of high occupancy at sites with the "SxE" motif associated with Fam20C, a major secretory pathway kinase [36–39]. The broad range of measured phosphosite occupancies indicates multi-faceted cellular regulation of neuropeptide phosphorylation.

Materials and Methods

Workflow

The workflow scheme in Figure 1 summarizes the approach of this study. DCSVs were isolated from bovine adrenal glands, lysed, and filtered through 10-kDa molecular weight cut-off (MWCO) membranes to separate the low MW peptides from large proteins. The peptide fraction was divided into two pools for the quantitative phosphatase experiments and the qualitative experiments utilizing immobilized metal affinity chromatography (IMAC). After LC-MS and bioinformatic analyses, all novel phosphosite IDs were combined with all phosphosites in the bovine Uniprot canonical protein sequence database (UP000009136) to compile a database of "verified phosphosites." This database was used for calculation of inferred phosphosite occupancy and can be found in Supplemental Information. All raw data is available at www.proteomexchange.com under PXD008064.

Materials

Protein measurements were conducted with the Bio-Rad DC protein assay kit (Hercules, CA). MWCO filters (10-kDa, MRCPRT010) were from Merck Millipore (Billerica, MA).

Sep-Pak solid-phase extraction (SPE) cartridges (WAT054955) and BEH C18 packing material (186004661) were from Waters Corporation (Milford, MA). The Pierce Colorimetric Total Peptide Assay (23275), Water (Optima, W6-4), acetonitrile (ACN, Optima, A955-4), formic acid (FA, Optima, A117-50), trifluoroacetic acid (TFA, Optima, A116-50), hydrochloric acid (HCl, A144-500), iodoacetamide (IAA, Acros Organics, 122270050), and FeCl3 (Acros Organics, 169430050) were from Thermo Fisher (Waltham, MA). Dithiothreitol (DTT, V3151) and Trypsin/LysC (V5073) were from Promega Corporation (Madison, WI). C18 material for SPE stage-tips (2215-C18) was from 3M (Maplewood, MN). Magnetic Ni-NTA beads (1007477) were from Qiagen (Hilden, Germany). Calf intestinal phosphatase (CIP, M0290S) was from New England Biolabs (Ipswich, MA).

Preparation of purified DCSV chromaffin granules from bovine adrenal medulla

Chromaffin granules were prepared from fresh adrenal medulla (bovine) by differential sucrose gradient centrifugation, optimized and conducted as described previously [40]. The purity of these isolated DCSV has been documented by electron microscopy and biochemical markers for subcellular organelles [41–43]. The sucrose density gradient purification results in intact DCSV that lack markers for lysosomes (acid phosphatase marker) [43], cytoplasm (lactate dehydrogenase marker) [42], mitochondria (fumarase and glutamate dehydrogenase markers) [41–42], and endoplasmic reticulum (glucose-phosphatase marker) [43]. Analysis of the purified DCSV through a second sucrose gradient revealed the lack of the lysosomal marker acid phosphatase, which further documented the purity of the isolated DCSV [40].

Endogenous peptide extraction

Peptide extraction methods were adapted and modified from our previously published, optimized protocol [18], and by protocols in the field [44]. Sixty milligrams of DCSV protein was divided into ten equal aliquots and diluted to volumes of 500 μL with MilliQ-filtered water. Next, aliquots were acidified by adding ice-cold HCl to 10 mM (pH ~2) and incubated on ice for 15 minutes. Precipitated protein was pelleted by $14,000 \times g$ microcentrifugation for 30 minutes at 4° C. Supernatants were then filtered through 10-kDa MWCO filters for 1 hour at 14,000 ×g, 4 °C. Finally, filtrates were desalted by C18 Sep-Pak SPE. Sep-Pak cartridges were equilibrated and washed with 0.1% TFA, and peptides were eluted with 40% ACN/0.1% TFA and 70% ACN/0.1% TFA. Elutions were dried down via speedvac and quantified by a colorimetric total peptide assay. The total DCSV peptide yield was approximately 450 μg.

Cysteine reduction and alkylation of peptides

Desalted peptides were resuspended in 8 M urea/50 mM TrisHCl (pH 8). Disulfide bonds were reduced by adding DTT to a sample concentration of 5 mM, followed by a 1 hour RT incubation. Reduced cysteines were then alkylated by adding IAA to a sample concentration of 15 mM, followed by a 30 minute RT incubation in the dark. Alkylation was quenched by adding a second aliquot of DTT equal to the volume of the first addition. The reduced and alkylated peptide pool was subsequently separated into two new pools with equal amounts of

total peptide. One pool was brought to 0.3% TFA and stored at −70 °C, and the other was digested by Trypsin/LysC.

Trypsin/LysC digestion

Samples were diluted with 50 mM TrisHCl (pH 8) so that the concentration of urea was less than 1 M. Trypsin/LysC was resuspended to a concentration of 0.5 μg/μL in 50 mM Tris-HCl and added to samples at a 50:1 peptide:enzyme ratio (w/w). Digests were then incubated at 37 °C for 24 hours, followed by acidification via TFA (pH ~2) and storage at −70 °C.

C18 stage-tip SPE

Following digestion and/or cysteine alkylation, peptides were desalted by self-fabricated C18 microcentrifuge state-tips [45]. Solvents for stage-tip equilibration, washing, and peptide elution were identical to those used with Sep-Pak SPE. Eluted peptides were dried via speedvac.

Iron-immobilized metal affinity chromatography (IMAC) phosphopeptide enrichment

One-hundred micrograms of Trypsin/LysC-digested and undigested DCSV peptides were removed from their respective peptide pools and resuspended in 500 μL 80% ACN/0.15% TFA. Two 75-μL aliquots of magnetic Ni-NTA bead slurry were washed three times with 1 mL of Optima-grade water. Then, the beads were suspended in 1 mL of 40 mM EDTA and mixed on a ThermoMixer (Thermo Fisher) for 30 minutes at 1000 rpm. Following three more washes with water, the beads were suspended in 1 mL of 100 mM $FeCl_3$ and mixed for 30 minutes at 1000 rpm. $FeCl_3$ was removed and beads were washed three times with 80% ACN/0.15% TFA. Peptide samples were then added to the iron-chelated beads and mixed for 30 min at 1000 rpm. Supernatants containing unbound peptides were removed and the beads were washed three times with 80% ACN/0.15% TFA. Bound peptides were subsequently eluted by adding 100 μL of 50% ACN/0.7% NH_4OH and vortexing for one minute. To prevent phosphate hydrolysis, the eluent was removed from the beads and immediately combined with 50 μL of 4% TFA. Phosphopeptides were then dried via speedvac and desalted with C18 stage-tips.

Alkaline Phosphatase (AP) treatment of peptides

One-hundred and twenty micrograms of the digested and undigested peptides that did not undergo IMAC enrichment were each resuspended in 1200 μL of AP buffer (100 mM NaCl, 50 mM Tris-HCl pH 7.9, 10 mM $MgCl_2$, 1 mM DTT) and divided into six 200-μL (20 μg) aliquots. Half of the aliquots received 12 μL (120 units) of CIP (calf intestinal phosphatase), and the other half received 12 μL of AP buffer alone as a no-phosphatase control. All of the aliquots were incubated at 37° C for two hours and subsequently quenched by acidification with TFA (pH ~2). Samples were then dried via speedvac and desalted with C18 stage-tips.

LC-MS analysis

All LC-MS was performed on a Dionex UltiMate 3000 nano LC and Orbitrap Q-Exactive mass spectrometer (Thermo Fisher). Samples were resuspended in 2% ACN/0.1% TFA.

Samples from AP experiments (+AP and −AP) were brought to a total peptide concentration of 667 ng/μL, and IMAC-enriched samples were brought to a total volume of 12 μL. For each analysis, 1 μL of sample was injected onto a self-fabricated nano LC column (75 μm ID, 360 μm OD, 25 cm length) with an integrated nanospray emitter. The column was packed with BEH C18 (1.7 μm diameter) solid-phase material and heated to 65 °C with a custom column heater. Details of the heater are reported elsewhere [46].

MS and tandem MS (MS/MS) spectra were recorded as a positive ion Top 12 data-dependent analysis. MS1 was acquired in profile mode with a 1e6 AGC target, 100 ms max injection time, 70000 resolution (at m/z 200), and a 350 to 1200 m/z window. MS2 was acquired in centroid mode with a 5e4 AGC target, 70 ms max injection time, 5e4 minimum precursor intensity, 15 second/10 ppm dynamic exclusion, 17500 resolution (at m/z 200), a first mass of m/z 150, and normalized HCD collision energy set to 27.

Each AP and no-AP sample was injected twice, and each IMAC sample was injected three times. A full technical report of the LC-MS method can be found in Supplemental Information. Raw files can be accessed at www.proteomexchange.org under the ID PXD008064.

Peptide identification

Peptides were identified by PEAKS (v 8.0) bioinformatic software [47]. Raw files were searched in four separate batches (digested IMAC samples, undigested IMAC samples, trypsin digested +AP/−AP samples, undigested +AP/−AP samples) against the Uniprot Bos taurus protein database (UP000009136, downloaded from www.uniprot.org on 08/01/2017). The results were then searched against a custom Neuropeptide Reference Database compiled from literature and online resources. A full summary of our Neuropeptide Reference Database and PEAKS search parameters can be found in Supplemental Information.

Peptide quantification

Label-free peptide quantification was performed by PEAKS. Features corresponding to peptide identifications were assigned an intensity based on the area of the precursor ion's LC peak. Match-between-runs mass and retention time shift tolerances were set to 9.0 ppm and 2.5 minutes, respectively. Normalization factors were omitted. Peptides were only quantified in +AP and −AP samples, and digested and undigested samples were quantified separately.

To minimize the number of low-quality features in our dataset, features were filtered by the following criteria. First, any feature whose amino acid sequence did not match to a peptide in the FDR-curated identification list were discarded. Then, features with a PEAKS Quality score less than 0.3, average area less than 1e4, confident identification in less than one-third of the raw files per batch, or less than three samples with non-zero intensities were also removed.

The filtered feature list was normalized with the Loess-G algorithm by Normalyzer [48]. Custom C# scripts were written to impute missing values and collapse the feature intensities from Normalyzer into peptide-level intensities. Details of these algorithms can be found in Supplemental Information.

Direct measurement of phosphosite occupancy

Phosphosite occupancy was calculated from a phosphopeptide's −AP sample intensities. If a phosphopeptide and its non-phosphorylated counterpart—a peptide with identical amino acid sequence and PTMs other than phosphorylation—was observed and quantified, occupancy is calculated as shown:

$$occupancy = \frac{I_{Phos}}{I_{Phos} + I_{NPC}} \times 100\%$$

I_{Phos}: intensity of phosphopeptide

I_{NPC}: intensity of non − phosphorylated counterpart

This method was adapted from Secher et al. [26]. If a phosphopeptide and its NPC are not both quantifiable, then direct site occupancy calculations were omitted.

Inferred phosphosite occupancy after AP-treatment of peptides

Inferred phosphosite occupancy was calculated by comparing peptide intensities in +AP and −AP samples. If the intensity of a non-phosphorylated peptide that overlaps with a verified phosphosite significantly increases after AP treatment, we assume that the increase came from peptides that were phosphorylated before treatment. Our study defines "verified phosphosites" as all known phosphosites in the Uniprot protein database for Bos taurus and any novel phosphosites we identified.

In the original method, Wu et al. used label-based peptide quantification [33] to calculate phosphosite occupancy. The label-free peptide quantification in this study does not provide the same level of precision. Consequently, we decided to use non-phosphorylated peptide intensity fold-change between +AP and −AP samples as a measure of relative phosphosite occupancy. Significantly high phosphosite occupancy required a Log_2(+AP/−AP) intensity ratio greater than 2.0 and a p-value less than 0.05 from a heterodescatic t-test.

Peptide-Averaged Endogenous Phosphosite (PEP) Intensity and Occupancy

Peptide-averaged Endogenous Phosphosite (PEP) intensities and occupancies of digested and undigested non-phosphorylated peptides were calculated as follows. First, all peptide intensities were converted to mean-normalized intensities. Next, non-phosphorylated peptides were organized into phosphosite groups based on their amino acid sequences. If two peptides from the same precursor overlapped the exact same verified phosphosites, they were placed in the same phosphosite group. PEP intensities for each group were then obtained by calculating the average mean-normalized intensity for each +AP and −AP replicate (+AP1, +AP2, +AP3; −AP1, −AP2, −AP3) across each peptide of the phosphosite group. PEP occupancy was obtained by taking the ratio of the Log_2-ratio of the mean +AP and −AP PEP intensities. A phosphosite was determined to have significantly high PEP

occupancy if displayed a Log_2(+AP/−AP) intensity ratio greater than 2.0 and p< 0.05 from a heterodescatic t-test.

Results and Discussion

In silico prediction of phosphosite motifs of prohormones and neuropeptides

Phosphorylation sites of bovine prohormones were compared to phosphosites on all bovine proteins by iceLogo sequence analyses (Figure 2.A.I.). These results showed the [S/T/Y]xE motif of prohormone phosphosites, which includes the SxE phosphosite motif of the secretory kinase Fam20C [36–39]. The prevalence of prohormone SxE phosphosite motifs was compared to previously identified phosphorylation sites of prohormones (Figure 2.A.II). The data shows the greater number of SxE motif sites compared to identified known SxE sites of prohormones. These findings indicate that many SxE phosphorylated sites of bovine prohormones have not been determined. Parallel analyses of human prohormones indicated the similar [S/T/Y]xE motifs present within human prohormones (Figure 2.B.I) and that many of these phosphosites have not yet been identified and characterized (Figure 2.B.II). Bovine and human prohormones show close similarities in phosphosite motifs, further verifying bovine prohormone-derived peptides as an accurate model for humans. These data predicted the identification of new and existing SxE phosphorylation sites on neuropeptides.

Peptide identification metrics of DCSV peptidomics data

Peptides identified by peptidomics analyses of the DCSV extract was conducted as shown in Figure 1 for alkaline phosphatase (AP) and IMAC experiments. Peptide-spectrum matches, unique peptides, proteins, protein groups, and unique phosphopeptide identifications were summarized in Table 1. The DCSV samples were very abundant in neuropeptides. The data showed that 57.8% of the undigested peptide IDs originated from known prohormones, and 37.4% directly overlapped with known neuropeptides. Additionally, we identified the intact forms of 30 endogenous peptides from the Neuropeptide Reference Database. A summary of these identifications and related extended/truncated IDs are shown in Table S1 (supplementary information).

DCSV phosphopeptide identification and phosphosite localization

Phosphopeptide identification occurred in both IMAC-enriched samples and +AP/−AP samples (Table 1). Other peptidomics studies have also observed phosphopeptides without IMAC enrichment [26–28]. Phosphopeptides comprised of 3.6% and 4.3% of the total undigested and digested +AP/−AP experiment identifications, respectively. In contrast, phosphopeptides comprised 56.0% of undigested and 66.1% of digested IMAC peptides.

Phosphopeptides and localized phosphosites were identified from many neuropeptide precursors and proteins across the DCSV peptidome (Figure 3A). Combining data from all experiments, a total of 118 unique non-redundant phosphosites were localized (AScore > 13), with 93 of those sites being novel identifications. Chromogranin B (CHGB) yielded the largest number of localized phosphosites, and multiple sites were localized on peptides derived from chromogranin A (CHGA), proenkephalin (PENK), secretogranin 2 (SCG2), adrenomedullin (ADM), proSAAS inhibitor of proprotein convertase 1 (PCSK1N),

secretogranin 5 (SCG5), and proneuropeptide Y (NPY) prohormones. The number of phosphosites shown includes localization of both single-residue and multi-residue sites. For example, T121 and S125 of chromogranin A (CHGA) each count as unique single-residue phosphosites. Data also showed the simultaneous phosphorylation of T121 and S125, which counts as an additional multi-residue phosphosite. Peptides with more than two phosphorylations were not identified.

The unique peptide identifications and overlap of localized single-residue phosphosites from experiments with and without trypsin digestion and/or IMAC enrichment are shown in Figure 3B. The IMAC-enriched samples yielded fewer total peptide IDs, but contributed a significant amount unique phosphosites. The reason for the low yield of phosphopeptides by IMAC may be due to the high content of acidic peptides of the chromogranins in DCSV (49, 50) which are known to bind to IMAC (51), and result in low phosphopeptide binding to IMAC as observed in this study. Overall, analyses of phosphopeptides benefits from using complementary combinations of IMAC, trypsin, and no digestion.

+AP versus –AP peptide quantification metrics

The metrics of peptide quantification in the undigested (Fig. 4A–B) and trypsin-digest (Fig. 4C–D) +AP/−AP samples are shown in Figure 4. The histograms in Figure 4A and Figure 4C display the expected normal distribution of +AP/−AP intensity ratios centered around 0.0 on a Log_2-scale. The volcano plots in Figure 4B and 4D further illustrates the pattern of intensity changes for phosphopeptides and non-phosphorylated peptides. The dotted-lines represent the thresholds for our significance criteria (Log_2(+AP/−AP) > 2 ‖ Log_2(+AP/−AP) < −2; p < 0.05). Phosphoserine, phosphothreonine, and unlocalized phosphopeptides are shown as green dots. Non-phosphorylated peptides are shown as blue dots. Phosphopeptides with a localized phosphotyrosine are shown as red dots. As expected, most phosphopeptides showed large intensity decreases after AP-treatment.

It was apparent that phosphotyrosine-containing peptides were not efficiently de-phosphorylated. Data analysis also suggests that the apparent inefficient de-phosphorylation of phosphotyrosine could be due to possible misidentification of sulfotyrosine (see supplemental information, Figure S2). A sulfotyrosine PTM differs from phosphotyrosine by only 0.005 Da and may not be distinguished by this data. For these reasons, phospho-Tyr was not included in further quantitative data analyses.

Overall, the quantification metrics were sufficient for alkaline phosphatase removal of phosphate groups from peptides to allow calculation of relative phosphopeptide stoichiometry and phosphosite occupancy for phosphopeptides without localized phosphotyrosine residues.

Direct phosphosite measurements of DCSV peptides leads to identification of putative novel phosphorylated neuropeptides

Results of this study indicate that a broad range of phosphosite occupancies were found on DCSV peptides. Table 2 shows the phosphosite occupancies of known endogenous peptides that were also identified as phosphopeptides in their intact forms. Although the C-terminal peptide of SCG5 does not have an established biological function, it displayed a phosphosite

occupancy greater than 98% on S204, a site with the SxE motif. Enkelytin, an anionic antimicrobial peptide derived from proenkephalin, was observed as both high and low occupancy unlocalized phosphopeptides at 77% and 10%. Intact forms of P01211(192–203). Secretolytin, and VIF displayed low occupancies in their intact forms.

Much of the high stoichiometric phosphorylation was observed on prohormone-derived peptides without known biological functions. The distribution of phosphosite occupancy across chromogranin B (CHGB) is shown in Figure 5. Data showed more phosphopeptides with site occupancy   90% from CHGB than any other neuropeptide precursor. The red and blue bars represent phosphopeptide IDs and their phosphosite occupancies from undigested samples. Phosphopeptides with high site occupancy were densely located within residues 162 to 206. Through closer inspection, we realized that one of these peptides, spanning residues 162–192, was located between dibasic prohormone processing sites, suggesting that this peptide CHGB (162–192) and may possess bioactivity. Interestingly, we identified phospho-CHGB (162–192) from both CHGB Uniprot sequence variants. The only difference between variants for residues 162–192 is a T181 for Uniprot entry P23389 and a M181 for Uniprot entry A0A140T885.

The highest direct measurements of phosphosite occupancy among all phosphopeptide IDs belong to CHGB (162–192) and its C-terminal extensions and truncations. The P23389 variants of CHGB (162–206), CHGB (162–188), CHGB (162–197), and the A0A140T885 variant of CHGB (162–192) displayed phosphosite occupancies over 99%, and the direct occupancy measurements of all phosphopeptides related to CHGB (162–192) ranged from 88.9% to 99.9%. Although our MS/MS was not sufficient to localize phosphorylation on the fully intact forms, the data localized phosphorylation to S168 on 24 other peptides that overlap portions of CHGB (162–192).

Inferred phosphosite occupancy increases depth of analysis

Inferred phosphosite occupancy measurements from +AP/−AP samples offered a powerful advantage over the direct method, as phosphosite occupancy can be measured without identifying phosphopeptides. However, there is an important distinction about the type of information gained from inferred versus direct measurement. For a given peptide overlapping multiple verified phosphosites, inferred measurements must be applied to all of them simultaneously. It is not possible to determine whether the +AP/−AP ratio represents occupancy for all the sites or just one of them.

In total, this investigation measured occupancy for 182 distinct single-residue phosphosites. Figure 6A shows a pie chart indicating the number of peptide phosphosites identified by the methods of direct, direct and inferred, and inferred only. Approximately 90.0% of site occupancies could only be measured via inferred methods, while only three site occupancies were uniquely measured with direct methods. This is further evidence of the added depth of the +AP/−AP approach in this study. In Figure 6B, a Venn diagram provides a breakdown of the phosphosite occupancies measured by only the inferred methods. The undigested samples and Trypsin/LysC digestion approaches are complementary and both provided significant contributions to the total number of quantified phosphosites.

Identifications of known neuropeptides that contain a verified phosphosite (highlighted in bold), as well as inferred phosphosite occupancy resulting from phosphatase analyses are shown in Table 3. Inferred phosphosite occupancy greatly enhanced the depth of these analyses. Phosphosite occupancy measured by Log_2(+AP/−AP) displayed very high to very low ratios, with the high values indicating the greatest phosphosite occupancy. Such values range from 10.36 for enkelytin to −0.30 for secretolytin. High occupancy was inferred for intact bioactive neuropeptides such as NPY, VIF, and enkelytin. Interestingly, high occupancies were observed for peptides without known bioactivities such as the C-flanking peptide of NPY, Manserin, and O62827 (153–188). Overall, neuropeptide phosphosite occupancy measured by both direct and inferred methods are complementary and enhance phosphopeptide occupancy analyses.

High-occupancy phosphorylation at S99 on VIF peptide indicated by peptide-averaged endogenous phosphosite (PEP) occupancy

VIF, a peptide from CHGA, was recently characterized as being able to inhibit angiotensin-induced vasoconstriction [5]. From inferred phosphosite occupancy measurements in the phosphatase experiments, intact VIF passed significance criteria with a Log_2(+AP/−AP) ratio of 2.79. Graphical analyses of overlapping VIF peptides are shown in Figure 7A. The profile suggests differential occupancy among VIF verified phosphosites. Phosphosite groups that contain S98 and S99 display large, significant +AP/−AP ratios, and none of the ratios from groups that do not include S98 or S99 are significant. Accordingly, the high phosphosite occupancy VIF residues is likely to be at S98 or S99.

To further justify the validity of the PEP method, we applied the same kind of analysis to PEP occupancy of phosphosite groups overlapped by enkelytin in Figure 7B. Enkelytin overlaps verified phosphosites S239, S245, and S247. If site occupancy is a good indicator of function, we would expect higher PEP occupancy for S245 and S247 because they are necessary for enkelytin's antimicrobial activity [7]. High occupancy of enkelytin peptide forms inferredwere, indeed, observed (Figure 7B).

High phosphosite occupancy and biological functions of endogenous peptides

Enkelytin is a well known DCSV neuropeptide whose biological function is highly dependent on phosphorylation. In the investigation by Goumon et al., it was shown that phosphorylation of S245 and S247 (previously referred to as S221 and S223) increased enkelytin's antimicrobial potency against *M. luteus* bacteria by nearly two orders of magnitude [7]. In the same report, the NMR analysis of non-phosphorylated enkelytin found S245 to be in close proximity to E252 when P251 was in a *trans*-conformation, while S247 was close to E254 with a *cis*-P251. Upon phosphorylation of S245 and S247, they hypothesized that electrostatic repulsion between phosphate and glutamate caused a conformation change that brought enkelytin to its active form.

In this study, PEP occupancy analysis of enkelytin's verified phosphosites indicated high phosphosite occupancy on peptides containing both S245 and S247, yet showed diminished occupancy on peptides that just contained S247. This data suggests that S245 phosphorylation is favored in DCSV, even though S247 is a Fam20C SxE motif. This

observation may reflect the proposed relationship of S245 and P251 *trans*-conformation, which is often slightly more energetically favorable than a *cis*-conformation [52]. Alternatively, low S247 PEP occupancy may represent this site's phosphorylation after proteolysis occurs between S245 and S247.

Experiments were unable to localize any of the undigested enkelytin-related phosphopeptide IDs, all of which were 20 residues or longer. In future experiments, use of alternative MS/MS fragmentation techniques, such as electron transfer dissociation (ETD) or activated ion-ETD, may assist in phosphosite localization for large phosphopeptide IDs with multiple potential sites [53].

In addition to enkelytin, high phosphosite occupancy occurred on other known bioactive neuropeptides. VIF appeared to have relatively high phosphorylation stoichiometry in its intact form, but it is unknown if phosphorylation will have a positive or negative effect on its activity. It is notable that high phosphosite occupancy was observed for endogenous peptides currently without a known function, such as C-terminal peptide from SCG5 and Manserin, as well as putative new peptides from unannotated regions of prohormones, such as CHGB (162–192). Future investigations should evaluate these peptides in their phosphorylated and non-phosphorylated forms to search for changes in bioactivity.

Clustering and iceLogo analyses of high occupancy phosphorylation sites reveals the SxE phosphosite motif of the Fam20C protein kinase

Among the 655 unique phosphopeptides directly identified in this study, 75.1% contained an SxE motif. Within the undigested phosphopeptides for which we directly calculated phosphorylation occupancy, 33 of the 37 peptides with occupancies greater than 50% also contained the motif. However, even among the phosphopeptides with occupancy below 50%, more than half were found to contain SxE.

Rigorous phosphosite motif analyses was conducted by hierarchical clustering and iceLogo analyses. PEP intensities of phosphosite groups were clustered by ClustViz [54] based on the Euclidean distances between their Log_2-transformed, mean-normalized intensities (Figure 8A). Each column on the heat map represents a unique, quantifiable phosphosite group, and each row corresponds to the group's PEP intensity for each +AP and −AP replicate. To minimize ambiguity over which residue contributed most to the observed +AP/−AP fold-change, only single-residue phosphosite groups were used for clustering. The heat map (Figure 8A) revealed three distinct clusters, labeled Cluster 1, Cluster 2, and Cluster 3. Cluster 1 included the largest positive Log_2(+AP/−AP) PEP intensity ratios and lower levels of inter-replicate variation. Cluster 3 was primarily made up of Log_2-PEP intensity ratios between 2.96 and 0.96, while Cluster 2 contained the lowest Log_2-ratios and no sites with significant PEP occupancy.

The iceLogo motif analyses of each phosphosite cluster is illustrated in Figure 8B. All amino acids appearing in the logo were significantly enriched from the background (8610 proteome-wide Ser/Thr *Bos taurus* phosphosites annotated by Uniprot) at $p < 0.1$, and those colored in red or blue enriched at $p < 0.05$. Cluster 1 and Cluster 3 show enrichment for the Fam 20C SxE motif, whereas the low PEP occupancy sites of Cluster 2 do not. Additionally,

the phosphosites of Cluster 2 appear to be under-enriched for other nearby serine residues. With respect to motif differences between Cluster 1 and Cluster 3, Cluster 1 appears to have an additional enrichment for glutamic residues in positions −1 to −3.

The results of the phosphosite hierarchical clustering and motif analyses suggests that high-occupancy phosphorylation is associated with the SxE motif, representing a strong predictor of prohormone phosphosites with high-occupancy. It is also noted that phosphosites without the SxE motif, such as S35 from HMGB1, T93 from ETFA, S98 from PEBP1, and S13 from PEBP1, had significantly high PEP occupancies. Furthermore, 16 phosphosites with the SxE motif were scattered throughout the low PEP occupancy Cluster 2. Overall, the SxE motif represents a major phosphosite motif (clusters 1 and 2) along with other motifs.

The SxE motif corresponds to the Fam20C protein kinase that has been investigated to represent a predominant protein kinase in the secretory pathway for secretion of proteins and peptides [36–38]. Results of this study showing the presence of the SxE phosphosite motif of prohormone-derived peptides suggests that Fam20C may participate in the regulated secretory pathway for stimulated secretion of DCSV neuropeptides. Fam20C has been detected in the lumen of Golgi fractions from which DCSV are generated. It will be of interest in future studies to investigate Fam20C and related protein kinases for phosphorylation of prohormone-derived peptides in the DCSV organelle for regulated secretion of neuropeptides.

Conclusion

Exploratory profiling of the phosphorylated DCSV peptidome in this study utilized direct and indirect methods to measure endogenous peptide phosphosite occupancy, an indicator of biological relevance. Overall, DCSV peptide phosphorylation displays a wide range of site occupancies. Many high-occupancy phosphosites were observed on peptides with no known function, although such phosphosites overlapped by peptides with known bioactivity, such as enkelytin and VIF, were also observed.

The data suggest differential regulation of neuropeptide phosphorylation within DCSVs, and is worthy of further study in biological systems. Release of neuropeptides with varying phosphosite occupancy into circulatory systems, synapses, or extracellular space is potentially a new mechanism for homeostatic maintenance or host defense response. Future investigations should involve knock-outs of Fam20C or removal of specific phosphosites using CRISPR [55]. The high phosphosite occupancies on peptides with no current function are interesting observations, and such approaches could help determine if their phosphorylation functions to process other bioactive peptides to maturity, or if they function as a secreted bioactive phosphopeptide.

Supplementary Material

Refer to Web version on PubMed Central for supplementary material.

Acknowledgments

References

1. Frederickson RC. Enkephalin pentapeptides--a review of current evidence for a physiological role in vertebrate neurotransmission. Life Sci. 1977; 21:23–42. [PubMed: 18645]

2. Hallberg M. Neuropeptides: metabolism to bioactive fragments and the pharmacology of their receptors. Med Res Rev. 2015; 35:464–519. [PubMed: 24894913]

3. Pedrazzini T, Pralong F, Grouzmann E. Neuropeptide Y: the universal soldier. Cell Mol Life Sci. 2003; 60:350–377. [PubMed: 12678499]

4. D'Amico MA, Ghinassi B, Izzicupo P, Manzoli L, Di Baldassarre A. Biological function and clinical relevance of chromogranin A and derived peptides. Endocr Connect. 2014; 3:R45–54. [PubMed: 24671122]

5. Salem S, Jankowski V, Asare Y, Liehn E, Welker P, Raya-Bermudez A, Pineda-Martos C, Rodriguez M, Muñoz-Castañeda JR, Bruck H, Marx N, Machado FB, Staudt M, Heinze G, Zidek W, Jankowski J. Identification of the "Vasoconstriction Inhibiting Factor" (VIF), a Potent Endogenous Cofactor of Angiotensin II Acting on the AT2 Receptor. Circulation, CIRCULATIONAHA. 2015:114.013168.

6. Troger J, Theurl M, Kirchmair R, Pasqua T, Tota B, Angelone T, Cerra MC, Nowosielski Y, Mätzler R, Troger J, Gayen JR, Trudeau V, Corti A, Helle KB. Granin-derived peptides. Prog Neurobiol. 2017; 154:37–61. [PubMed: 28442394]

7. Goumon Y, Lugardon K, Kieffer B, Lefèvre JF, Van Dorsselaer A, Aunis D, Metz-Boutigue MH. Characterization of antibacterial COOH-terminal proenkephalin-A-derived peptides (PEAP) in infectious fluids. Importance of enkelytin, the antibacterial PEAP209–237 secreted by stimulated chromaffin cells. J Biol Chem. 1998; 273:29847–29856. [PubMed: 9792701]

8. Metz-Boutigue MH, Goumon Y, Strub JM, Lugardon K, Aunis D. Antimicrobial chromogranins and proenkephalin-A-derived peptides: Antibacterial and antifungal activities of chromogranins and proenkephalin-A-derived peptides. Ann N Y Acad Sci. 2003; 992:168–178. [PubMed: 12794056]

9. Brogden KA, Guthmiller JM, Salzet M, Zasloff M. The nervous system and innate immunity: the neuropeptide connection. Nat Immunol. 2005; 6:558–564. [PubMed: 15908937]

10. Shooshtarizadeh P, Zhang D, Chich JF, Gasnier C, Schneider F, Haikel Y, Aunis D, Metz-Boutigue MH. The antimicrobial peptides derived from chromogranin/secretogranin family, new actors of innate immunity. Regul Pept. 2010; 165:102–110. [PubMed: 19932135]

11. Hook V, Funkelstein L, Lu D, Bark S, Wegrzyn J, Hwang SR. Proteases for processing proneuropeptides into peptide neurotransmitters and hormones. Annu Rev Pharmacol Toxicol. 2008; 48:393–423. [PubMed: 18184105]

12. Hook V, Bandeira N. Neuropeptidomics Mass Spectrometry Reveals Signaling Networks Generated by Distinct Protease Pathways in Human Systems. J Am Soc Mass Spectrom. 2015; 26:1970–1980. [PubMed: 26483184]

13. Lippincott-Schwartz J, Roberts TH, Hirschberg K. Secretory protein trafficking and organelle dynamics in living cells. Annu Rev Cell Dev Biol. 2000; 16:557–589. [PubMed: 11031247]

14. Hammel I, Lagunoff D, Galli SJ. Regulation of secretory granule size by the precise generation and fusion of unit granules. J Cell Mol Med. 2010; 14:1904–1916. [PubMed: 20406331]

15. Albrethsen J, Goetze JP, Johnsen AH. Mining the granule proteome: a potential source of endocrine biomarkers. Biomark Med. 2015; 9:259–265. [PubMed: 25731211]

16. Hook V, Bark S, Gupta N, Lortie M, Lu WD, Bandeira N, Funkelstein L, Wegrzyn J, O'Connor DT, Pevzner P. Neuropeptidomic Components Generated by Proteomic Functions in Secretory Vesicles for Cell–Cell Communication. AAPS J. 2010; 12:635–645. [PubMed: 20734175]

17. Bark SJ, Wegrzyn J, Taupenot L, Ziegler M, O'Connor DT, Ma Q, Smoot M, Ideker T, Hook V. The protein architecture of human secretory vesicles reveals differential regulation of signaling molecule secretion by protein kinases. PLoS One. 2012; 7:e41134. [PubMed: 22916103]

18. Gupta N, Bark SJ, Lu WD, Taupenot L, O'Connor DT, Pevzner P, Hook V. Mass Spectrometry-Based Neuropeptidomics of Secretory Vesicles from Human Adrenal Medullary Pheochromocytoma Reveals Novel Peptide Products of Prohormone Processing. J Proteome Res. 2010; 9:5065–5075. [PubMed: 20704348]

19. Campbell DJ, Krum H, Esler MD. Losartan increases bradykinin levels in hypertensive humans. Circulation. 2005; 111:315–320. [PubMed: 15655136]

20. Jimenez CR, Spijker S, de Schipper S, Lodder JC, Janse CK, Geraerts WP, van Minnen J, Syed NI, Burlingame AL, Smit AB, Li K. Peptidomics of a single identified neuron reveals diversity of multiple neuropeptides with convergent actions on cellular excitability. J Neurosci. 2006; 26:518–529. [PubMed: 16407549]

21. Lee HK, Zhang L, Smith MD, Walewska A, Vellore NA, Baron R, McIntosh JM, White HS, Olivera BM, Bulaj G. A marine analgesic peptide, Contulakin-G, and neurotensin are distinct agonists for neurotensin receptors: uncovering structural determinants of desensitization properties. Front Pharmacol. 2015; 6:11. [PubMed: 25713532]

22. Humphrey SJ, James DE, Mann M. Protein phosphorylation: a major switch mechanism for metabolic regulation. Trends Endocrinol Metab. 2015; 26:676–687. [PubMed: 26498855]

23. Johnson LN. The regulation of protein phosphorylation. Biochem Soc Trans. 2009; 37:627–641. [PubMed: 19614568]

24. Baldwin G, Knesel J, Monckton J. Phosphorylation of gastrin-17 by epidermal growth factor-stimulated tyrosine kinase. Nature. 1983; 301:435–437. [PubMed: 6600511]

25. Bishop L, Dimaline R, Blackmore C, Deavall D, Dockray GJ, Varro A. Modulation of the cleavage of the gastrin precursor by prohormone phosphorylation. Gastroenterology. 1998; 115:1154–1162. [PubMed: 9797370]

26. Secher A, Kelstrup CD, Conde-Frieboes KW, Pyke C, Raun K, Wulff BS, Olsen JV. Analytic framework for peptidomics applied to large-scale neuropeptide identification. Nat. Commun. 2016; 7:11436. [PubMed: 27142507]

27. Frese CK, Boender AJ, Mohammed S, Heck AJR, Adan RAH, Altelaar AFM. Profiling of Diet-Induced Neuropeptide Changes in Rat Brain by Quantitative Mass Spectrometry. Anal Chem. 2013; 85:4594–4604. [PubMed: 23581470]

28. Sasaki K, Osaki T, Minamino N. Large-scale identification of endogenous secretory peptides using electron transfer dissociation mass spectrometry. Mol Cell Proteomics. 2013; 12:700–709. [PubMed: 23250050]

29. Romanova EV, Sweedler JV. Peptidomics for the discovery and characterization of neuropeptides and hormones. Trends Pharmacol Sci. 2015; 36:579–586. [PubMed: 26143240]

30. Li L, Sweedler JV. Peptides in the Brain: Mass Spectrometry–Based Measurement Approaches and Challenges. Annu Rev Anal Chem. 2008; 1:451–483.

31. Carmichael SW, Winkler H. The adrenal chromaffin cell. Sci Am. 1985; 253:40–49. [PubMed: 3161180]

32. Winkler H. The adrenal chromaffin granule: a model for large dense core vesicles of endocrine and nervous tissue. J Anat. 1993; 183(Pt 2):237–252. [PubMed: 8300414]

33. Wu R, Haas W, Dephoure N, Huttlin EL, Zhai B, Sowa ME, Gygi SP. A large-scale method to measure absolute protein phosphorylation stoichiometries. Nat Meth. 2011; 8:677–683.

34. Olsen JV, Mann M. Status of Large-scale Analysis of Post-translational Modifications by Mass Spectrometry. Mol Cell Proteomics. 2013; 12:3444–3452. [PubMed: 24187339]

35. Colaert N, Helsens K, Martens L, Vandekerckhove J, Gevaert K. Improved visualization of protein consensus sequences by iceLogo. Nat Meth. 2009; 6:786–787.

36. Tagliabracci VS, Engel JL, Wen J, Wiley SE, Worby CA, Kinch LN, Xiao J, Grishin NV, Dixon JE. Secreted kinase phosphorylates extracellular proteins that regulate biomineralization. Science. 2012; 336:1150–1153. [PubMed: 22582013]

37. Tagliabracci VS, Pinna LA, Dixon JE. Secreted protein kinases. Trends Biochem Sci. 2013; 38:121–130. [PubMed: 23276407]

38. Tagliabracci, Vincent S., Wiley, Sandra E., Guo, X., Kinch, Lisa N., Durrant, E., Wen, J., Xiao, J., Cui, J., Nguyen, KB., Engel, JL., Coon, JJ., Grishin, N., Pinna, LA., Pagliarini, DJ., Dixon, JE. A Single Kinase Generates the Majority of the Secreted Phosphoproteome. Cell. 2015; 161:1619–1632. [PubMed: 26091039]

39. Sreelatha A, Kinch LN, Tagliabracci VS. The secretory pathway kinases. Biochim Biophys Acta. 2015; 1854:1687–1693. [PubMed: 25862977]

40. Wegrzyn JL, Bark SJ, Funkelstein L, Mosier C, Yap A, Kazemi-Esfarjani P, La Spada AR, Sigurdson C, O'Connor DT, Hook V. Proteomics of dense core secretory vesicles reveal distinct protein categories for secretion of neuroeffectors for cell-cell communication. J Proteome Res. 2010; 9:5002–5024. [PubMed: 20695487]

41. Smith AD, Winkler H. A simple method for the isolation of adrenal chromaffin granules on a large scale. Biochem J. 1967; 103:480–482. [PubMed: 6032982]

42. Gratzl M, Krieger-Brauer H, Ekerdt R. Latent acetylcholinesterase in secretory vesicles isolated from adrenal medulla. Biochim Biophys Acta. 1981; 649:355–366. [PubMed: 7317405]

43. Hook VY, Eiden LE. Two peptidases that convert 125I-Lys-Arg-(Met)enkephalin and 125I-(Met)enkephalin-Arg6, respectively, to 125I-(Met)enkephalin in bovine adrenal medullary chromaffin granules. FEBS Lett. 1984; 172:212–218. [PubMed: 6378657]

44. Che F-Y, Zhang X, Berezniuk I, Callaway M, Lim J, Fricker LD. Optimization of Neuropeptide Extraction from the Mouse Hypothalamus. J Proteome Res. 2007; 6:4667–4676. [PubMed: 17979226]

45. Rappsilber J, Mann M, Ishihama Y. Protocol for micro-purification, enrichment, pre-fractionation and storage of peptides for proteomics using StageTips. Nat Protocols. 2007; 2:1896–1906. [PubMed: 17703201]

46. Richards AL, Hebert AS, Ulbrich A, Bailey DJ, Coughlin EE, Westphall MS, Coon JJ. One-hour proteome analysis in yeast. Nat Protocols. 2015; 10:701–714. [PubMed: 25855955]

47. Zhang J, Xin L, Shan B, Chen W, Xie M, Yuen D, Zhang W, Zhang Z, Lajoie GA, Ma B. PEAKS DB: De Novo Sequencing Assisted Database Search for Sensitive and Accurate Peptide Identification. Mol Cell Proteomics. 2012; 11 M111.010587.

48. Chawade A, Alexandersson E, Levander F. Normalyzer: A Tool for Rapid Evaluation of Normalization Methods for Omics Data Sets. J Proteome Res. 2014; 13:3114–3120. [PubMed: 24766612]

49. Taupenot L, Harper KL, O'Connor DT. The chromogranin-secretogranin family. N Engl J Med. 2003; 348:1134–49. [PubMed: 12646671]

50. Estevez-Herrera J, Pardo MR, Dominguez N, Pereda D, Machado JD, Borges R. The role of chromogranins in the secretory pathway. Biomol Concepts. 2013; 4:605–9. [PubMed: 25436760]

51. Thingholm TE, Larsen MR. Phosphopeptide enrichment by immobilized metal affinity chromatography. Methods Mol Biol. 2016; 1355:123–33. [PubMed: 26584922]

52. Wedemeyer WJ, Welker E, Scheraga HA. Proline Cis–Trans Isomerization and Protein Folding. Biochemistry. 2002; 41:14637–14644. [PubMed: 12475212]

53. Riley NM, Hebert AS, Dürnberger G, Stanek F, Mechtler K, Westphall MS, Coon JJ. Phosphoproteomics with Activated Ion Electron Transfer Dissociation. Anal Chem. 2017; 89:6367–6376. [PubMed: 28383256]

54. Metsalu T, Vilo J. ClustVis: a web tool for visualizing clustering of multivariate data using Principal Component Analysis and heatmap. Nucleic Acids Res. 2015; 43:W566–W570. [PubMed: 25969447]

55. Hay EA, Knowles C, Kolb A, MacKenzie A. Using the CRISPR/Cas9 system to understand neuropeptide biology and regulation. Neuropeptides. 2017; 64:19–25. [PubMed: 28038787]
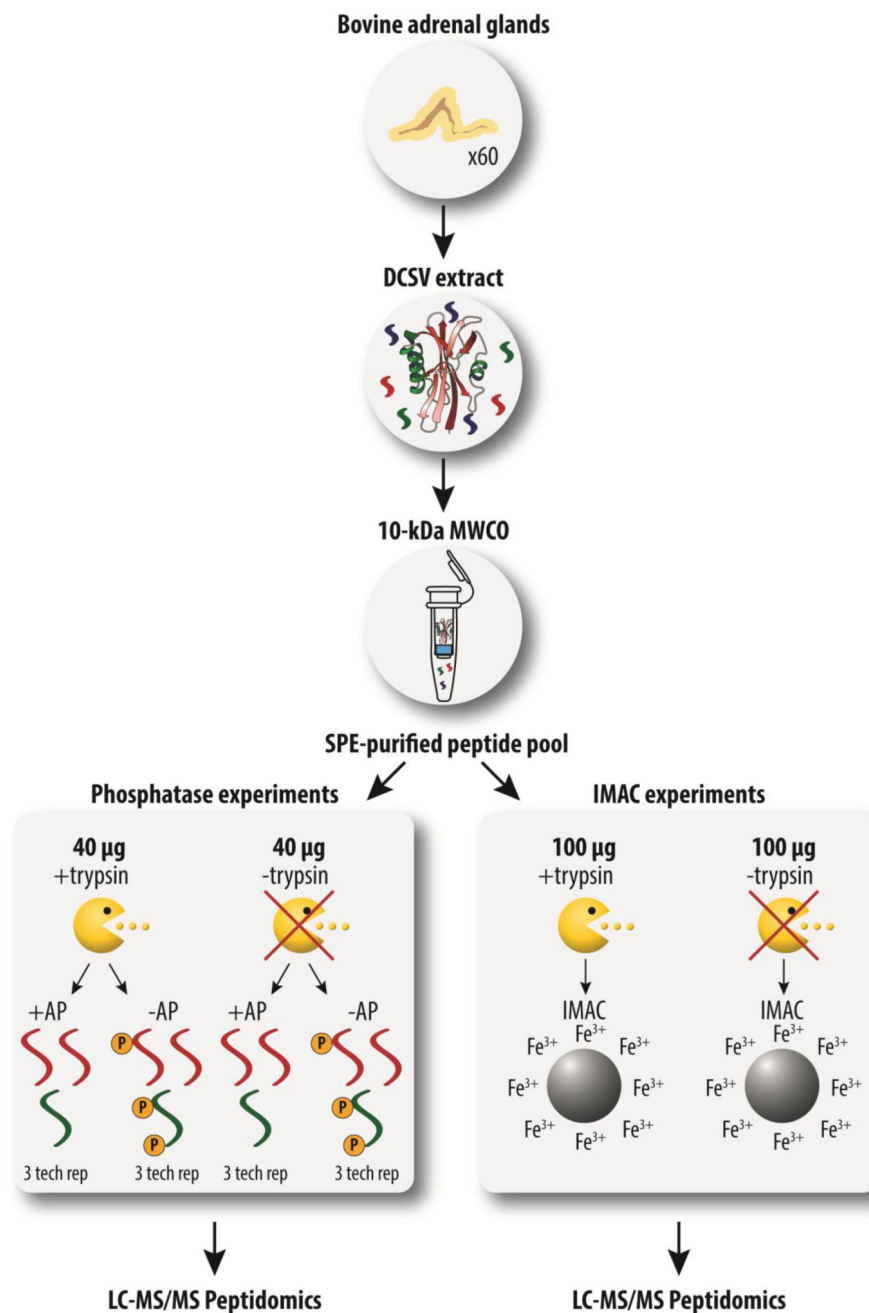
Figure 1. Workflow of DCSV peptidomics and phosphopeptidomics
A purified peptide pool from bovine adrenal cell DCSVs was split for quantitative phosphatase experiments that utilize alkaline phosphatase (+AP) and no AP (−AP) treatments and qualitative phosphopeptide enrichment experiments (IMAC). Phosphosite occupancy was directly measured by intensity comparisons of phosphopeptides and their non-phosphorylated counterparts in −AP samples. Occupancy was also inferred by the intensity differences of non-phosphorylated peptides between +AP and −AP samples.
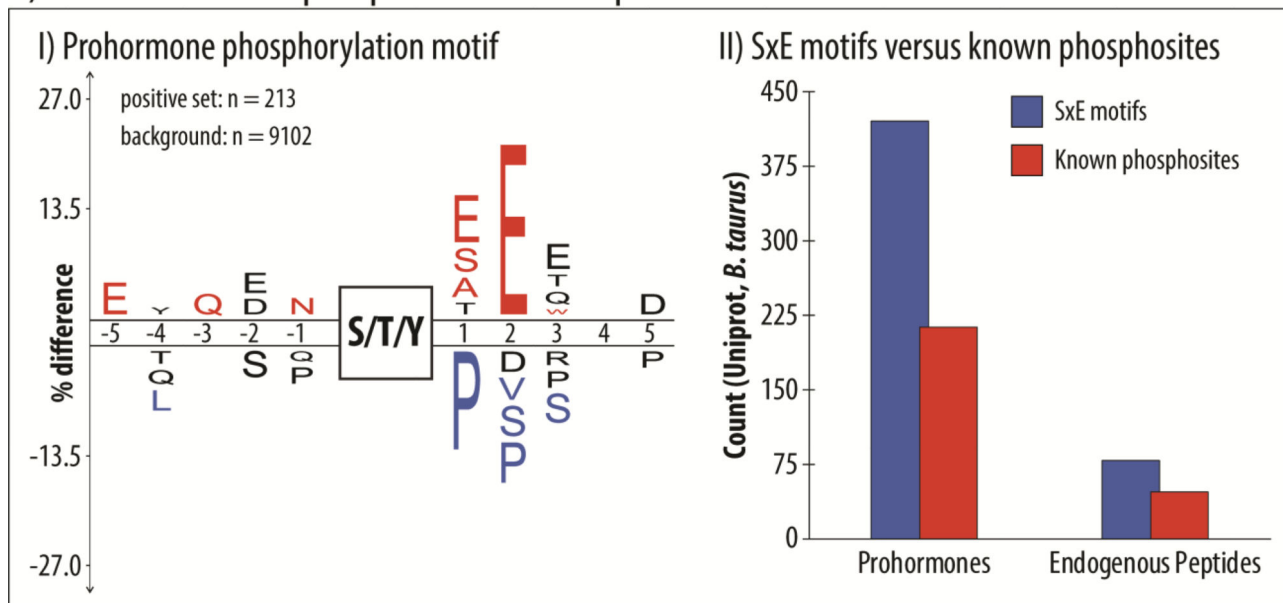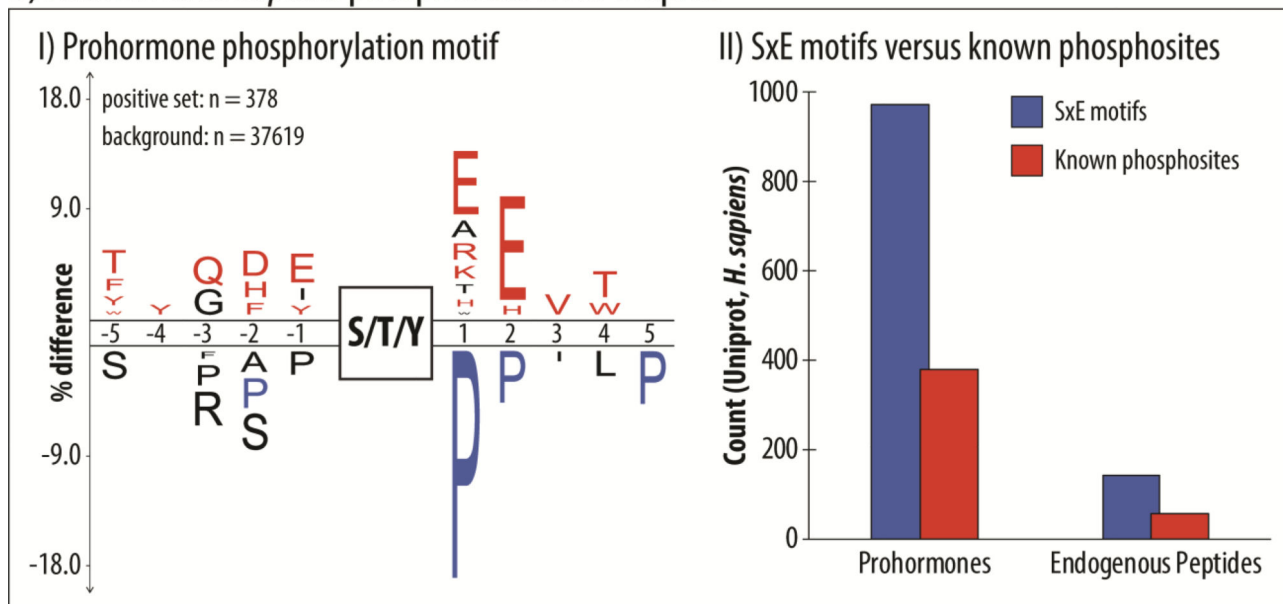
Figure 2. *In silico* analysis of known prohormone and endogenous peptide phosphorylation
A.I.) iceLogo amino acid motif analysis of phosphosites on bovine prohormones. The background set consisted of all known phosphosites among all proteins in the Uniprot canonical protein sequence database for *Bos taurus* (UP000009136). The positive set consisted of the phosphosites on bovine prohormones. Percent-differences of residues in black are at a significance level of $p < 0.1$, while residues in red and blue are significant at $p < 0.05$. A.II.) Bar charts show the number of SxE phospho site motifs of prohormones and endogenous peptides compared to the number of known (identified) phosphosites in the Uniprot protein database for *B. taurus*. In B.I and B.II, parallel analyses of human

prohormones and endogenous peptides from all reviewed proteins in the Uniprot canonical protein sequence database for *Homo sapiens* (UP000005640) are shown.
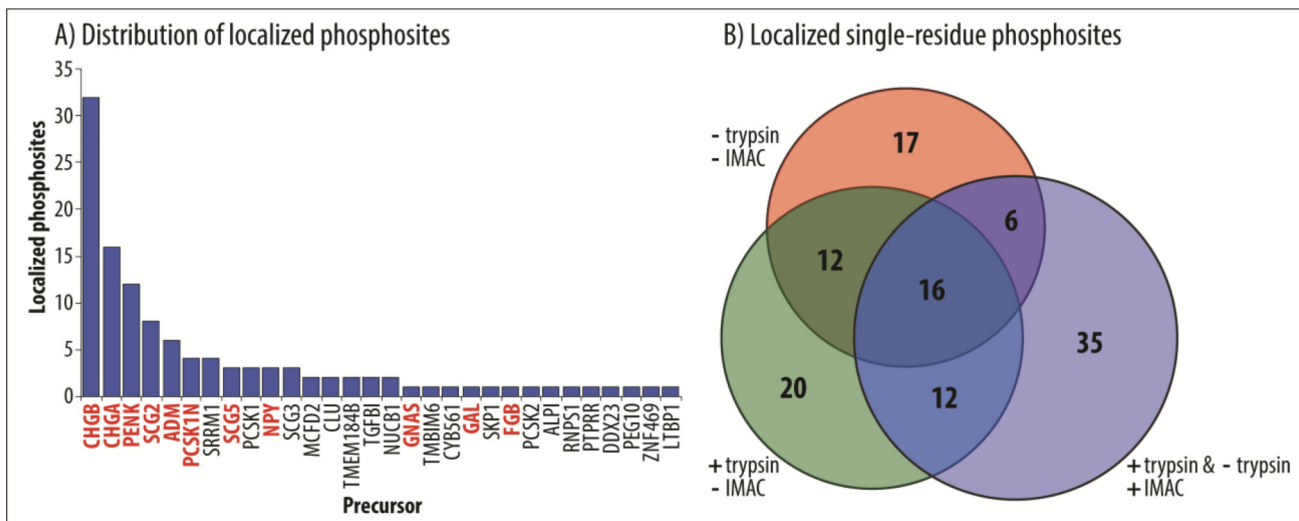
Figure 3. Phosphosite localization on DCSV peptides

A) Distribution of localized phosphosites—unambiguous identification of the phosphorylated residue on a phosphopeptide (AScore 13)—on peptides from various neuropeptide and protein precursors. The Y-axis represents the number of unique single-residue and multi-residue phosphosite localizations per precursor. Precursors in red denote known prohormones. B) The Venn diagram shows the overlap of single-residue phosphosite localization in each experiment. Results from digested and undigested IMAC-enrichments were combined into a single dataset (blue circle).
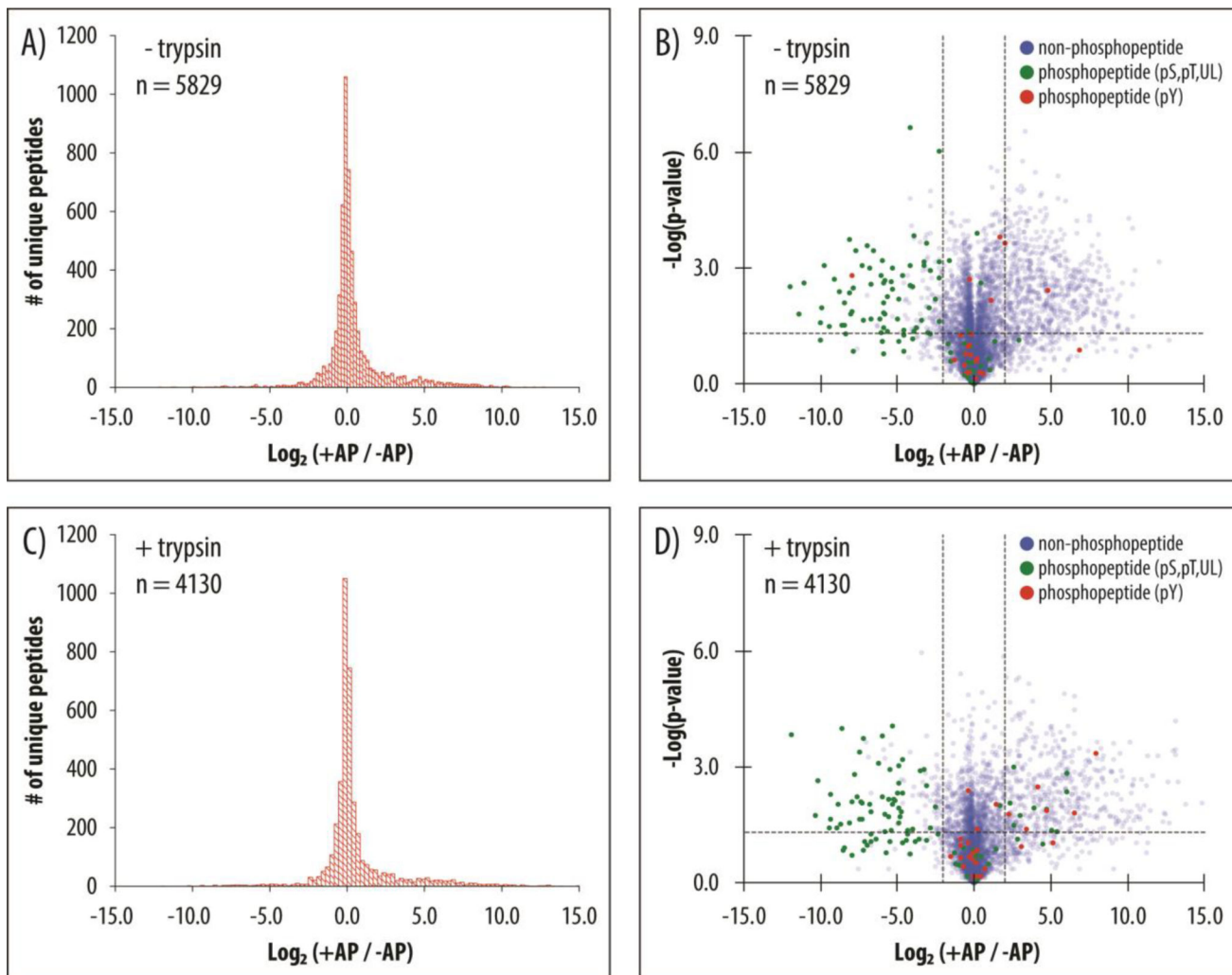
Figure 4. Peptide quantification metrics in +AP/−AP experiments

A) Log$_2$(+AP/−AP) intensity ratio histogram for all quantifiable undigested peptides. B) Plot of −Log$_{10}$(p-value) versus Log$_2$(+AP/−AP) for all quantifiable undigested peptides. Blue dots denote non-phosphorylated peptides; green dots denote localized phosphoserine (pS), phosphothreonine (pT), and unlocalized (UL) phosphopeptides; and red dots denote localized phosphotyrosine phosphopeptides. The dotted lines denote significance thresholds [Log$_2$(+AP/−AP) > +2.0 ‖ Log$_2$(+AP/−AP) < −2.0; p < 0.05]. C) and D) contain parallel histograms and scatter plots for tryptic peptides.
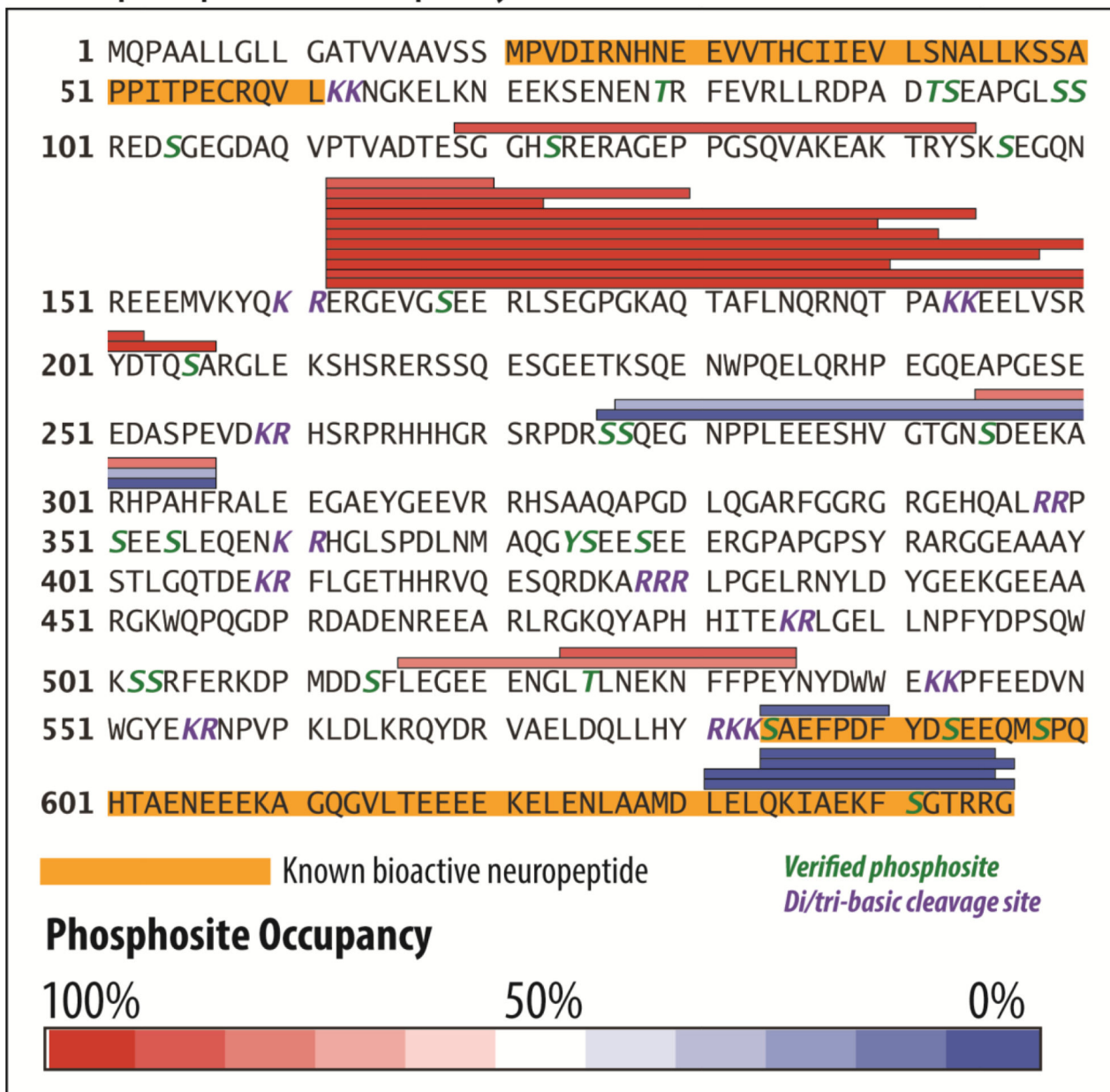
Figure 5. Direct phosphosite occupancy measurements for chromogranin B (CHGB)
A) Colored bars represent endogenous phosphopeptide IDs and their location in the prohormone sequence. The color of the bar denotes phosphosite occupancy, calculated by comparison of its intensity to that of its non-phosphorylated counterpart by direct measurements (in −AP samples). Residues in green denote verified phosphosites. Residues in purple denote di/tri-basic cleavage sites for endogenous DCSV proteases. Neuropeptides with established bioactivity originate from CHGB regions highlighted in yellow.
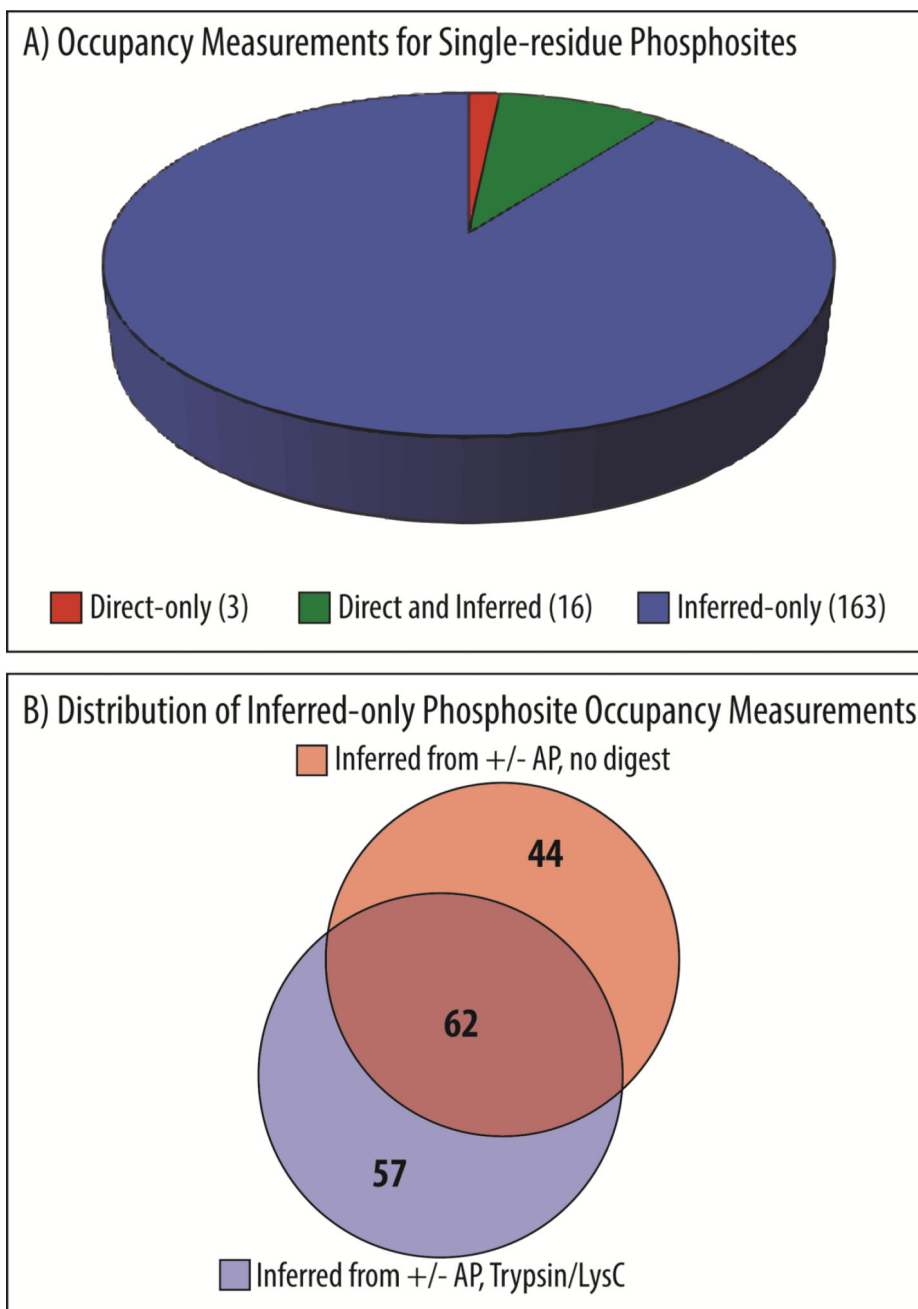
Figure 6. Distribution of phosphosite occupancy measurements by direct and inferred methods
A) A pie chart displays the direct only, direct and inferred, and inferred only methods
utilized for phosphosite occupancy measurements for each of the 182 single-residue
phosphosites that were identified and quantified in this study. Red indicates that occupancy
was only measured directly, blue indicates that occupancy was only be inferred through +/−
AP experiments, and green indicates site occupancies that were measured with both
methods. B) A Venn diagram of single-residue phosphosite occupancies that could only be
measured by inferred methods shows the overlap of site occupancies measured from intact
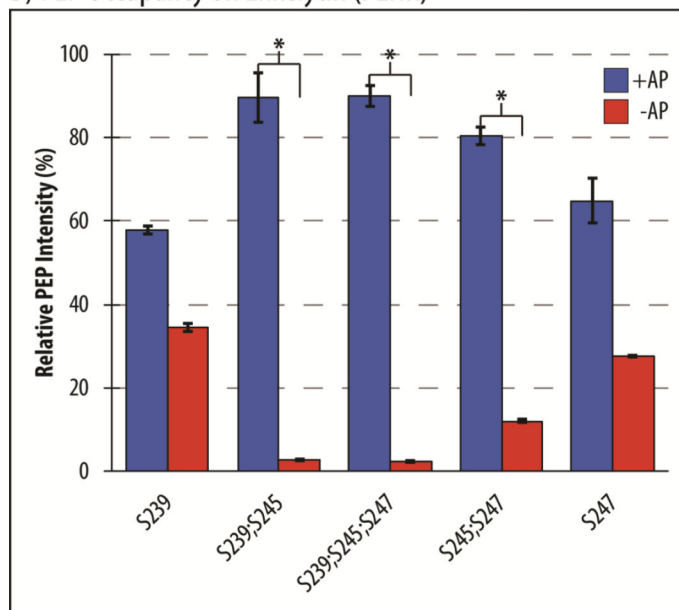endogenous peptides (no digest) and tryptic peptides (Trypsin/LysC).
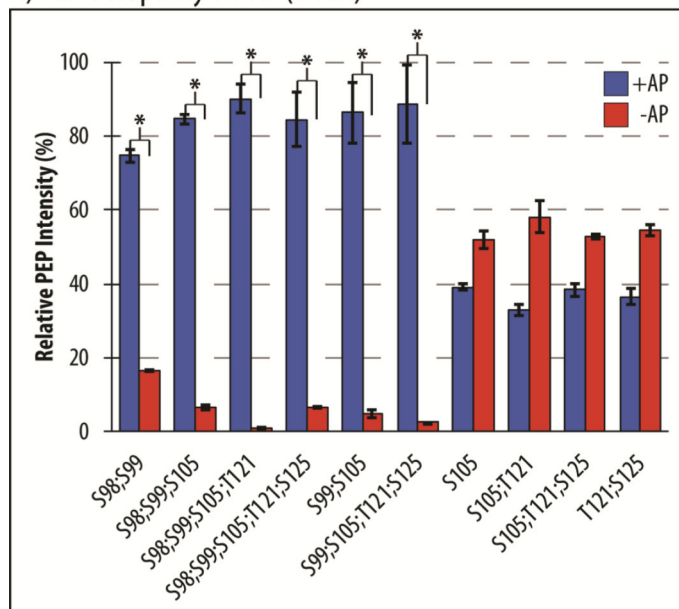
Figure 7. PEP (peptide-averaged endogenous phosphosite) intensity and occupancy on VIF and enkelytin

Relative +AP (blue) and −AP (red) PEP intensities of verified phosphosites on A) VIF and B) Enkelytin. VIF peptide is residues 97–131 of the chromogranin A (CHGA) precursor. Enkelytin peptide is residues 233–261 of the proenkephalin (PENK) precursor. PEP intensity was normalized to largest intensity observed among all sites listed. Error bars represent standard error of the mean. An asterisk (*) indicates that the Log_2(+AP/−AP) > 2.0 and p-value < 0.05.

A) Hierarchical clustering of PEP intensity for single-residue phosphosites
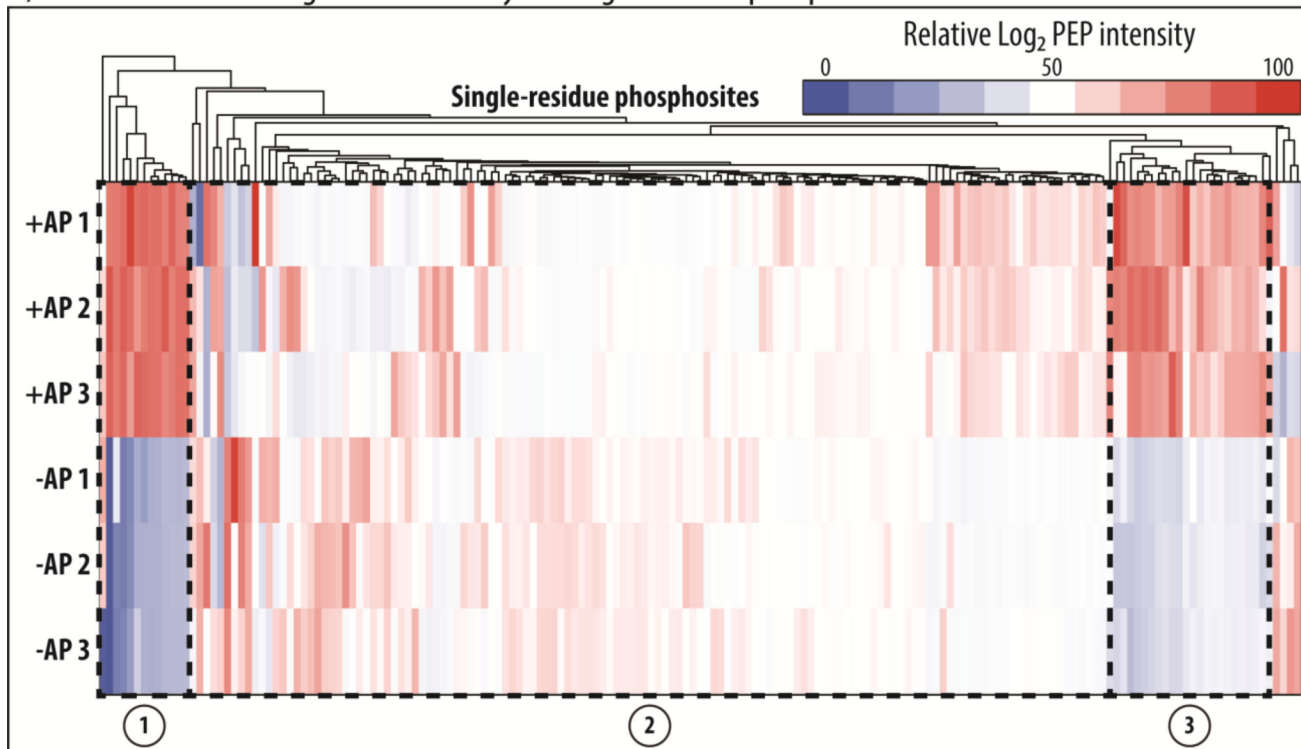
B) Phosphosite Ice-Logo analysis of PEP clusters
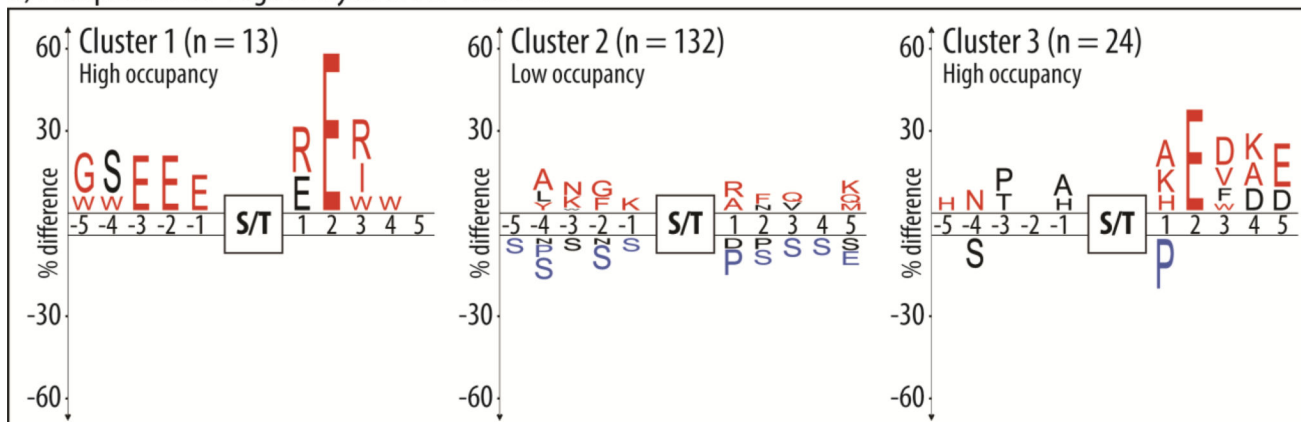
Figure 8. Hierarchical clustering of PEP intensity and phosphosite iceLogo analysis

A) Hierarchical clustering of single-residue Peptide-averaged Endogenous Phosphosite (PEP) intensity. Each column represents a single-residue phosphosite, and each row/color denotes the Log_2-scale mean-normalized PEP intensity within +AP and −AP experimental replicates. Sites were clustered according to the Euclidean distances between intensities from each +AP and −AP experiment. B) iceLogo analysis of all phosphosites from PEP clusters in A). The background set consisted of all annotated Uniprot *Bos taurus* phosphosites, as detailed in Figure 1. Percent differences of residues in black are significant at $p < 0.1$, while residues in red and blue are significant at $p < 0.05$. The percent difference

represents the change in frequency of an amino acid in the dataset vs. all known bovine phosphosite motifs.

Table 1

Peptide Identification Metrics

Summary of peptide-spectrum-match (PSM), unique peptide, protein, protein group (proteins collapsed into indistinguishable protein identifications), and phosphopeptide identifications in each group of experiments.

Experiment	Trypsin	PSMs (%FDR)	Unique Peptides (% FDR)	Unique Proteins/Groups (% FDR)*	Unique Phosphopeptides (% total)
AP	–	68114 (0.1)	7361 (0.9)	680/530 (0.9)	264 (3.6)
AP	+	47154 (0.1)	5224 (0.9)	905/715 (0.9)	226 (4.3)
IMAC	–	404 (0.2)	191 (0.5)	27/18 (0.0)	107 (56.0)
IMAC	+	1554 (0.4)	514 (0.9)	21/19 (0.0)	340 (66.1)

*
FDR was calculated at the protein-level

Table 2

Direct Identification and Calculation of Phosphosite Occupancy for Prohormone-Derived Peptides

Summary of phosphosite occupancies for known endogenous peptides, calculated by comparison of phosphopeptide intensity with intensity of its non-phosphorylated counterpart. Bold and underlined residues indicate a localized residue (AScore > 13). Multiple entries for the same sequences are due to multiple, distinct phosphopeptides. Lowercase "m" indicates oxidized methionine.

Name	Sequence	Gene	Localized*	Occupancy (%)
C-terminal peptide	SVPHF**S**DEDKDPE	SCG5		98.7
Enkelytin	FAEPLPSEEEGESYSKEVPEmEKRYGGFm	PENK		77.0
Enkelytin	FAEPLPSEEEGESYSKEVPEmEKRYGGFm	PENK		10.3
VIF	HSSYEDELSEVLEKPNDQAEPKEV**T**EEVSSKDAAE	CHGA		4.7
P01211(192–203)	**S**PHLEDETKELQ	PENK		0.3
Secretolytin	QKIAEKFSGTRRG	CHGB		0.1
P01211(192–203)	SPHLEDE**T**KELQ	PENK		0.02

*Refers to phosphosite localization on intact peptide sequence—localization may have been achieved on related extensions and fragments. Peptide phosphosite occupancy was determined by the direct method of LC-MS/MS.

Table 3

Inferred Phosphosite Occupancy on Intact Peptides Derived from Prohormones

Summary of inferred phosphosite occupancy intensity ratios $Log_2(+AP/-AP)$ calculated for the intact forms of known endogenous peptides overlapping at least one verified phosphosite (bold, highlighted). Inferred phosphosite occupancy is calculated from non-phosphorylated peptides. Additional modifications are indicated: oxidized methionine (m), pyroglutamate (q), carbamidomethylation (c), C-term amidation (a), and N-term acetylation (Ac−).

Name	Sequence	Gene	$Log_2(+AP/-AP)$	p-val
Enkelytin	FAEPLP**S**EEEGE**SYS**KEVPEMEKRYGGFM	PENK	10.36[*]	0.018
C-flanking pep. of NPY	SSPETLISDLLmRE**ST**GNIPRTRLEDPSmW	NPY	9.26[*]	0.015
Enkelytin	FAEPLP**S**EEEGE**SYS**KEVPEMEKRYGGFm	PENK	8.22[*]	0.048
Enkelytin	FAEPLP**S**EEEGE**SYS**KEVPEmEKRYGGFm	PENK	8.18[*]	0.001
Enkelytin	FAEPLP**S**EEEGE**SYS**KEVPEmEKRYGGFM	PENK	8.05	0.140
PENK(233–254)	FAEPLP**S**EEEGE**SYS**KEVPEME	PENK	7.81[*]	0.042
PENK(233–254)	FAEPLP**S**EEEGE**SYS**KEVPEmE	PENK	7.73[*]	0.037
C-flanking pep. of NPY	SSPETLISDLLMRE**ST**GNIPRTRLEDPSmW	NPY	7.35[*]	0.010
O62827(153–188)	**S**LPEAGLGRTLLQPPPEPKLRGAPD**S**RVHQVLATLRI	ADM	6.75[*]	0.008
Manserin	VPSQG**S**TEDDRQDENQIEQALKEHLSQH**SS**QETDKLASVS	SCG2	6.67[*]	0.010
C-terminal peptide	SVPHF**S**DEDKDPE	SCG5	5.99[*]	0.022
Neuropeptide Y	YPSKPDNPGEDAPAEDLARYYSALRHYINLI**T**RQRYa	NPY	5.17[*]	0.004
GE-25	GWRPN**S**RED**S**VEAGLPLQVRGYPEE	CHGA	4.61	0.130
VIF	H**SS**YEDEL**S**EVLEKPNDQAEPKEV**T**EEV**S**SKDAAE	CHGA	2.79[*]	0.035
P011211(192–203)	Ac-**S**PHLEDE**T**KELQ	PENK	1.18	0.034
PENK(140–179)	DAEEDDGLGNSSNLLKELLGAGDQREG**S**LHQEG**S**DAEDV**S**	PENK	1.04	0.019
Adrenomedullin-11–26	LR**S**FGcRFG**T**c**T**VQKL	ADM	0.17	0.392
Secretolytin (NTE)	DLELQKIAEKF**S**GTRRG	CHGB	0.07	0.873
SCG5 Peptide 1	**S**VNPYLQGQRLDNVVA	SCG5	−0.07	0.798

Name	Sequence	Gene	Log$_2$(+AP/−AP)	p-val
Little LEN	LE**T**PAPQAPA	PCSK1N	−0.10	0.044
Secretolytin	qKIAEKF**S**GTRRG	CHGB	−0.15	0.047
P01211(192–203)	**S**PHLEDE**T**KELQ	PENK	−0.17	0.006
Secretolytin	QKIAEKF**S**GTRRG	CHGB	−0.30	0.031
O62827(45–92)	ELRESSSYPTGLADVKAGPVQTLIRPQDVKGA**S**RSPQASSPDAARIRV	ADM	−0.34	0.010

*
Log$_2$(+AP/−AP) > 2.0, p-value < 0.05